

# Expanding Conjugate Space of RNAi Therapeutics: Ligand at the 3' End of the Antisense Strand Achieves Uncompromised In Vivo Potency and Efficacy and Reveals Interactions with the Argonaute-2 PAZ Domain

Rajat S. Das, Dhruvjayoti Datta, Christopher R. Brown, Jason A. Gilbert, Amy Chan, Jennifer Willoughby, Swati Gupta, MaryBeth Kim, Rohan Degaonkar, Tim Racie, Li Lei, Mark K. Schlegel, Adam Castoreno, Klaus Charisse, Kallanthottathil G. Rajeev, Martin Egli, and Muthiah Manoharan\*



Cite This: *J. Med. Chem.* 2025, 68, 4397–4409



Read Online

ACCESS |



Metrics & More

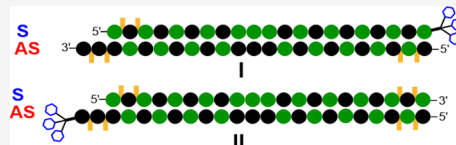


Article Recommendations



Supporting Information

**ABSTRACT:** The conjugation of the sense strands of small interfering RNA (siRNA) to tri-*N*-acetylgalactosamine (GalNAc), the ligand for a hepatocyte-specific receptor, enables the delivery of multiple clinically approved therapeutic agents that act through the RNA interference pathway. Here, we report the systematic evaluation of siRNAs with the 3' termini of antisense strands conjugated to GalNAc for the first time. These designs retained the same receptor affinity, in vitro and in vivo activities, as well as the same level of loading into the RNA-induced silencing complex as siRNAs with a GalNAc-conjugated sense strand. A siRNA with a GalNAc-conjugated antisense strand of 22 nucleotides had better activity than a siRNA with a 23-nucleotide antisense strand. Computational modeling of a complex of a GalNAc-conjugated antisense strand with the PAZ domain of Ago2 rationalizes the importance of the interaction of phosphate at the 3' terminus with the PAZ domain to explain the observed activity of these siRNAs.



## INTRODUCTION

Therapeutics that act through the RNA interference (RNAi) pathway prevent the production of disease-causing proteins by downregulating the corresponding mRNAs.<sup>1–3</sup> Synthetic small interfering RNA (siRNAs), which induce gene silencing via the endogenous RNAi process, must be chemically modified to limit nuclease degradation, facilitate their cellular uptake through the cell membrane, and reduce their immune stimulation.<sup>4,5</sup> When the sense strand of the siRNA is conjugated to tri-*N*-acetylgalactosamine (GalNAc; Figure 1A,C), the ligand for the asialoglycoprotein receptor (ASGPR), which is highly expressed on hepatocytes, siRNAs are specifically delivered into the liver.<sup>6–9</sup> The sense strands of four of the five clinically approved liver hepatocyte-targeting siRNAs from Alnylam<sup>6,7,10–14</sup> and another approved siRNA from Dicerna<sup>15</sup> as well as several siRNAs in clinical trials have a GalNAc at the 3'-end of the sense strand.<sup>16</sup>

As the antisense strand mediates targeting of the RNA-induced silencing complex (RISC) to the complementary mRNA, it has been assumed that bulky modifications of this strand would be detrimental, and few chemical modifications have been evaluated at the 3' end of the antisense strand.<sup>17–22</sup> One report demonstrated that a 2'-*O*-methyl (2'-*OME*) at the 3' terminal position of the antisense strand impairs activity.<sup>23</sup> Although 3'-sense and 3'-antisense conjugates with mono-

valent GalNAc moieties of valencies 1 through 4 were evaluated in vitro for silencing activity, only sense-strand conjugates were preferred for the evaluation in animal models.<sup>24</sup>

Here, we demonstrated that siRNAs in which the 3' terminus of the antisense strand is conjugated to triantennary GalNAc through a hydroxyprolinol linker are as potent in vitro and in vivo as siRNAs in which the conjugation to GalNAc is on the 3' end of the sense strand (Figure 1A,B). This observation was confirmed by targeting three mRNAs, namely, *Ttr*, *C5*, and *FXII*. We showed that activities correlated with in vivo liver exposure and RISC loading. We also evaluated siRNAs with DNA versus 2'-*OME* and with phosphorothioate (PS) versus phosphodiester at the 3' terminus of the GalNAc-conjugated antisense strand. Activities were evaluated in cell culture under transfection conditions, which are indicative of intrinsic potency, and in the absence of transfection reagent, which requires transport into cells through ASGPR, and in

**Received:** September 20, 2024

**Revised:** November 29, 2024

**Accepted:** December 27, 2024

**Published:** February 3, 2025



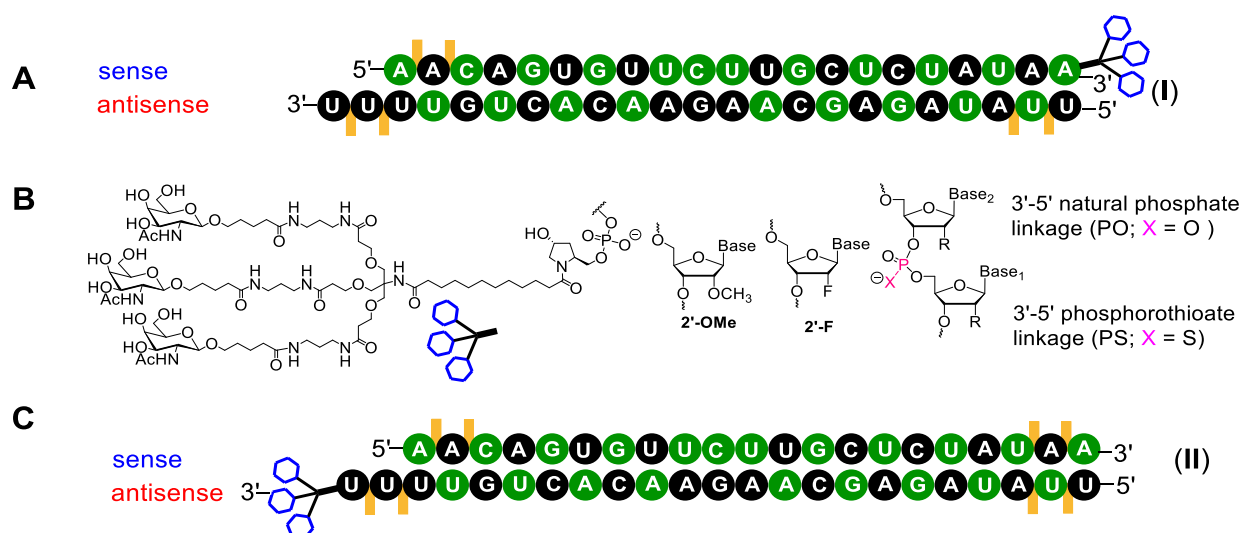


**Figure 1.** (A, C) Schematics of siRNAs with GalNAc conjugated at (A) the 3' end of the sense strand and (C) the 3' end of the antisense strand. 2'-Fluoro (2'-F) and 2'-O-methyl (2'-OMe) nucleotides are indicated in green and black, respectively. Phosphorothioate (PS) linkages are indicated by orange lines. (B) Chemical structure of the GalNAc ligand used in this study and structures of 2'-OMe, 2'-F, natural phosphate linkage, and PS linkage.

mice. Potency was similar for all siRNAs, indicating that conjugation of a ligand to the antisense strand is a viable strategy. Further, we established that an siRNA duplex with a 21-nucleotide sense strand and a 22-nucleotide antisense strand, the latter conjugated to the GalNAc ligand, was a potent design. Computer modeling of the interaction of an antisense strand with a 3'-terminal GalNAc with the PAZ domain of Argonaute (Ago2) revealed productive interactions between 3' phosphate, linker, and ligand with the PAZ domain. A single-stranded oligonucleotide with a 3'-terminal GalNAc and a 5' vinylphosphonate was inactive in vitro and in mice. These data based on ligand binding affinity, in vitro and in vivo silencing results, quantitative Ago2-drug loading, and computer modeling indicate that double-stranded siRNAs with 3' antisense-strand conjugates should be pursued clinically.

## RESULTS

### GalNAc Conjugation at the 3' End of the Antisense Strand Does Not Impair the ASGPR Binding Affinity.

siRNAs targeting mouse *Ttr* mRNA (siRNAs I and II), *C5* mRNA (siRNAs III and IV), and *FXII* mRNA (siRNAs V and VI) were prepared with GalNAc conjugated to the 3' ends of the sense strands or to the 3' ends of the antisense strands (Tables 1 and S1). siRNAs with sense strand conjugation to GalNAc, which is the typical design used in several FDA-approved siRNAs, contained six phosphorothioate (PS) linkages and were chemically modified as described earlier.<sup>9</sup> siRNAs with antisense strand conjugation contained eight PS linkages and were otherwise modified exactly as were their sense-strand conjugated counterparts. To verify that the 3' antisense conjugation strategy did not impact binding to the ASGPR on the cell surface of hepatocytes, we measured the binding affinities of the GalNAc-conjugated siRNAs to ASGPR expressed on these cells using a fluorescence-based binding assay.<sup>25</sup> Binding affinities were the same within experimental error for siRNAs with the GalNAc conjugated to the 3' termini of antisense strands and for those with conjugation to the sense strands (Figure 2, Table 1).

### GalNAc Conjugation at the 3' End of the Antisense Strand Does Not Impair Silencing In Vitro.

Next, RNAi-mediated silencing of expression from *Ttr*, *C5*, and *FXII* mRNAs was evaluated in primary mouse hepatocytes when siRNAs were transfected into cells or by free uptake. No significant differences in transfection or free uptake activities were observed when siRNAs with GalNAc at the 3' end of the sense strand and GalNAc at the 3' end of the antisense strand were compared (Tables 1 and S2). In addition, the removal of two PS linkages from the overhang connecting GalNAc to the 3' end of the antisense strand did not impact potency under transfection or free uptake conditions (Table 1 and S2) as siRNAs with six versus eight PS linkages had comparable activities (for *Ttr* II vs VII; for *C5* IV vs XVII; and for *FXII* VI vs XVIII; Table S2). These experiments with siRNAs targeting three different mRNAs demonstrate that there is no difference in inherent potency or cellular uptake for siRNAs with GalNAc on the 3' sense or 3' antisense strand and that removal of terminal PS linkages in the 3' antisense GalNAc siRNAs does not reduce in vitro silencing activity.

### GalNAc Conjugation at the 3' End of the Antisense Strand Does Not Impair Silencing In Vivo.

We previously showed that a *Ttr*-targeted siRNA conjugated with GalNAc on the 3' end of the sense strand (I) significantly reduces levels of circulating TTR protein in mice.<sup>7</sup> We compared the activity of this siRNA to the siRNA with GalNAc on the 3' end of the antisense strand (II). Mice were dosed subcutaneously at 1 mg/kg, and levels of circulating TTR protein were measured at 7, 14, 21, and 28 days postdose. Treatment with the two siRNAs resulted in comparable levels of TTR protein reduction over the course of time (Figure 3). Similarly, siRNAs targeting *C5* with GalNAc conjugated to sense or to antisense strands (III and IV, respectively) had comparable potencies at day 5 following a 1 mg/kg subcutaneous dose (Figure S1). As the siRNAs with an antisense strand conjugated to GalNAc have eight PS linkages but the siRNAs with a sense strand conjugated to GalNAc have only six PS linkages, we also tested an siRNA targeting *Ttr* that has a sense strand conjugated to GalNAc and that has eight PS linkages

Table 1. GalNAc Conjugation at the 3' Terminus of the Antisense Strand Does Not Impair Silencing In Vitro

Duplex ID	S/AS (number of nt) <sup>[b]</sup>	siRNA duplex sequences <sup>[c]</sup>	Target <sup>[a]</sup>	K <sub>i</sub> [nM] <sup>[d]</sup>	IC <sub>50</sub> [nM] <sup>[e]</sup>		
					Transfection	Free uptake	
I	S (21) AS (23)		Ttr	51.1 ± 8.6	0.0451	0.1023	
II	S (21) AS (23)			24.1 ± 2.7	0.0368	0.1074	
VII	S (21) AS (23)			n.d.	0.0497	0.1414	
VIII	S (21) AS (23)			n.d.	0.162	0.134	
IX	S (21) AS (23)			n.d.	0.069	0.286	
X	S (21) AS (23)			n.d.	0.072	0.139	
XI	S (22) AS (22)			n.d.	0.068	0.116	
XII	S (22) AS (23)			n.d.	0.042	0.045	
XIII	S (21) AS (21)			n.d.	0.015	0.059	
XIV	S (21) AS (22)			n.d.	0.108	0.250	
XV	S (21) AS (25)			n.d.	n.d.	n.d.	
XVI	S (21) AS (25)			n.d.	n.d.	n.d.	
III	S (21) AS (23)			C5	43.8 ± 4.8	0.1129	0.130
IV	S (21) AS (23)				44.0 ± 4.9	0.0358	0.116
XVII	S (21) AS (23)				n.d.	0.0794	0.127
VI	S (21) AS (23)			FXII	34.7 ± 9.7	0.937	0.776
XVIII	S (21) AS (23)		n.d.		0.821	4.169	
V	S (21) AS (23)		42.9 ± 5.0		0.972	0.881	
XIX	AS (23) 13 PS	5'-VP-UUUUUGGACUUUUUUGGAGAGAUU-3'	Ttr single- strand designs	n.d.	120.62	n.d.	
XX	AS (23) 14 PS	5'-VP-UUUUUGGACUUUUUUGGAGAGAUU-3'		n.d.	65.11	n.d.	

<sup>a</sup>siRNAs target mRNAs encoding mouse TTR, C5, or FXII. <sup>b</sup>S and AS indicate sense and antisense strands, and nt indicates nucleotides. <sup>c</sup>Bead diagrams of tested siRNAs. 2'-F, 2'-OME, DNA nucleotides are indicated in green, black, and blue, respectively. PS linkages are indicated by orange lines. Top and bottom sequences are sense and antisense, respectively. <sup>d</sup>Binding affinities for ASGPR on primary mouse hepatocytes. n.d. indicates not determined. <sup>e</sup>Half maximal inhibitory concentration (IC<sub>50</sub>) for in vitro gene silencing under transfection (Lipofectamine RNAiMAX) or free uptake conditions in primary mouse hepatocytes. n.d. indicates not determined.

(siRNA VIII). This siRNA did not differ in potency from the siRNA that has a sense strand conjugated to GalNAc but has only six PS linkages (Figure 3). These results in mice confirm our in vitro observations that there is no difference in potency of siRNAs conjugated with GalNAc on the 3' termini of the sense or antisense strands and further indicate that the addition of two additional PS residues on the 3' end of the sense strand does not adversely impact activity. Furthermore, a good correlation between in vitro and in vivo silencing results (shown below) was observed, except where the in vivo conditions cause loss of metabolic stability with 3'-antisense overhang phosphodiester containing siRNA VII. In this case, siRNA VII and VIII have similar in vitro activities but different in vivo activities, as discussed in the next section.

**Phosphorothioate Linkages Stabilize 3' Antisense Strand GalNAc Conjugates In Vivo.** Terminal PS linkages are necessary to stabilize the siRNA strands against exonuclease activity. As GalNAc is conjugated to the 3' end of the antisense strand through a *trans*-4-hydroxyprolinol linker, we speculated that the linker and the bulky ligand would protect this strand from degradation by nucleases.<sup>9</sup> Indeed, our in vitro results indicated that the two 3'-terminal PS linkages were not necessary (Table 1). We tested this in vivo by comparison of the *Ttr*-targeting siRNA II, which has eight PS linkages, to siRNA VII, which has six; siRNA VII does not have PS linkages at the 3' end of the antisense strand. Mice were treated subcutaneously with 1 mg/kg siRNA II or 0.5, 1, or 2.5 mg/kg siRNA VII, and levels of circulating TTR protein

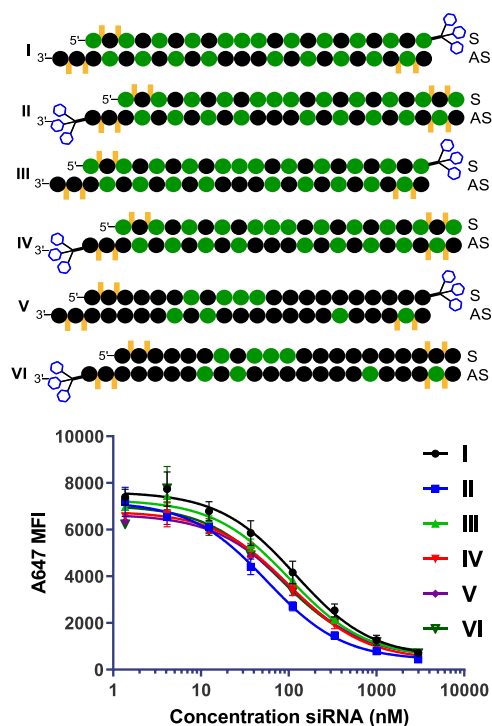


**Figure 2.** Affinity for ASGPR is not compromised by conjugation of GalNAc to the antisense strand. Upper: Bead diagrams of the siRNAs. The first siRNA in the pair has triantennary GalNAc at the 3' end of the sense strand, and the second has the GalNAc at the 3' end of the antisense strand. Lower: Affinity for ASGPR as a function of siRNA concentration as measured by mean fluorescence intensity in fluorescence-based binding assay for siRNAs I (black) and II (blue) targeting *Ttr*, III (green) and IV (red) targeting *C5*, and V (violet) and VI (dark green) targeting *FXII*. Mean  $\pm$  standard deviations of three biological replicates are plotted.  $K_i$  values are reported in Tables 1 and S2.

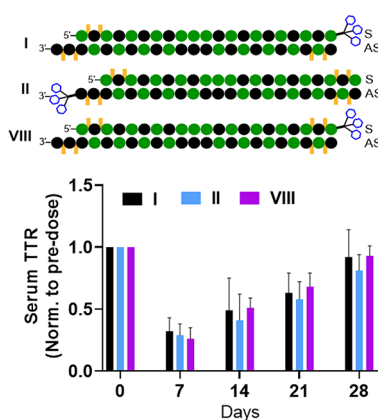


**Figure 3.** siRNAs with GalNAc conjugated to the 3' end of the sense strand and to the 3' end of the antisense strand have equivalent potencies in mice. Upper: Bead diagrams of the tested siRNAs. Lower: TTR protein quantified by ELISA in serum of mice treated subcutaneously with 1 mg/kg of siRNA I (black), II (blue), or VIII (violet) and normalized relative to predose TTR levels. Means  $\pm$  standard deviations are plotted ( $n = 3$  per group).

were analyzed by ELISA predose and at days 4, 7, 10, 14, and 21 postdose. At 1 mg/kg, siRNA II was more efficacious than siRNA VII; the maximum TTR protein reduction was 75% for siRNA II and only 40% for siRNA VII. Moreover, siRNA II

had a longer duration of action than siRNA VII (Figure 4). At 2.5 mg/kg, the highest dose evaluated for siRNA VII,

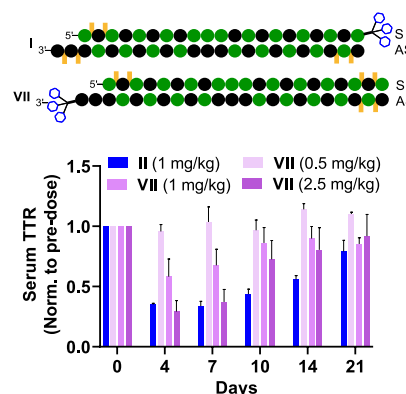


**Figure 4.** Phosphorothioate linkages at the 3' terminus of the antisense strand are necessary for high potency. Upper: Bead diagrams of tested siRNAs. Lower: Serum TTR protein was quantified by ELISA in mice treated with 1 mg/kg siRNA II (blue) or 0.5 mg/kg (light violet), 1.0 mg/kg (violet), or 2.5 mg/kg (dark violet) siRNA VII. Data were normalized relative to predose TTR levels. Mean  $\pm$  standard deviations are plotted ( $n = 3$  per group).

approximately 75% reduction in TTR was observed on days 4 and 7 and only about 25% reduction was observed on day 10 postdose. The direct comparison between siRNAs II and VII suggests that the two additional PS linkages at the 3' terminus of the antisense strand are stabilizing in vivo. This difference was not observed in vitro, suggesting that the environment in vivo is harsher than that observed in vitro. Considering the free overhang with two nucleotides, more stabilization through the addition of two phosphorothioates is required to protect the 3' terminus from nucleases.

**siRNA Potency Correlates with Liver Exposure and RISC Loading.** Ago2 associates with the 5' end of the antisense strand via its MID domain and with the 3' end of the antisense strand through its PAZ domain.<sup>26,27</sup> Alterations in the structure of either of these ends can affect loading and subsequent gene silencing efficiency,<sup>18–22,24</sup> and, therefore, we examined the impact of conjugation of GalNAc to the 3' end of the antisense strand on liver stability, loading into Ago2, and formation of functional RISC complexes. We treated mice subcutaneously with 1 mg/kg siRNA. At 5 days postdose, siRNA II, with GalNAc conjugated to the antisense strand and eight PS linkages caused 63% reduction in *Ttr* mRNA in the liver compared to predose levels; this reduction is similar to the reductions resulting from treatment with siRNA I and siRNA VIII (67 and 61%, respectively), which have GalNAc conjugated to the 3' end of the sense strand (Figure 5A). As expected based on its lower potency in vivo, siRNA VII, which is the antisense strand conjugate with only six PS linkages, did not reduce *Ttr* mRNA in the liver on day 5. Moreover, there were considerably lower levels of siRNA VII in the liver compared to the other tested siRNAs (Figure 5B), and the Ago2 loading of this siRNA, determined according to a published procedure,<sup>28</sup> was very low (Figure 5C).

To validate the broad utility of this approach, a similar experiment was performed with siRNAs targeting *C5*. The siRNA with GalNAc on the 3' end of the sense strand, siRNA III, was compared to siRNAs IV and XVII, which have GalNAc on the antisense strand and eight and six PS linkages,

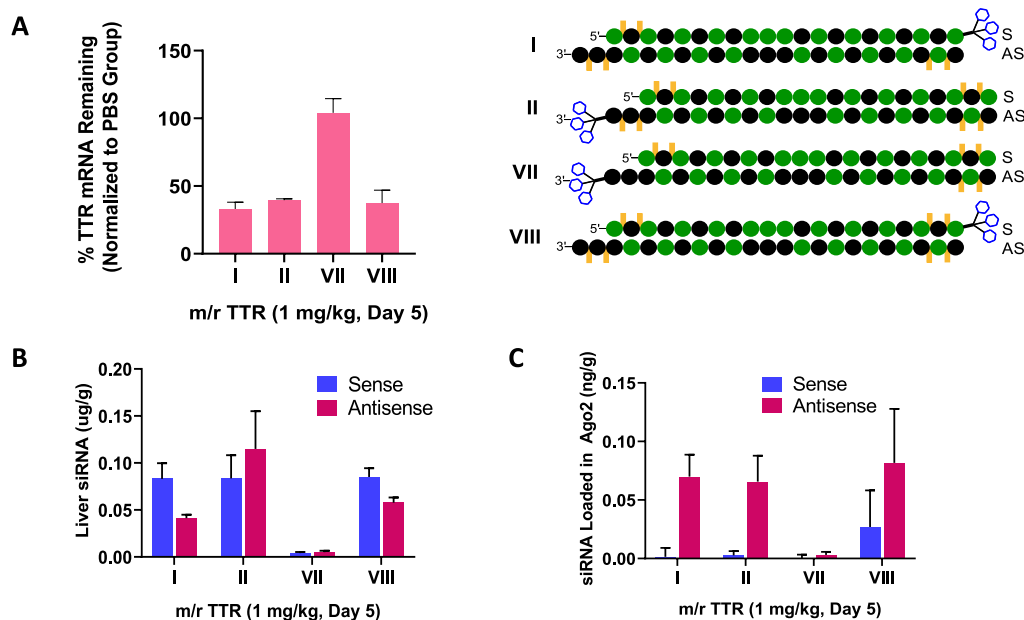


**Figure 5.** Phosphorothioate linkages at the 3' end of the antisense strand enhance liver exposure. (A–C) Mice were treated subcutaneously with 1 mg/kg of siRNAs I, II, VII, or VIII, and livers were collected on day 5. (A) Left: Percent *Ttr* mRNA remaining. Right: Bead diagrams of tested siRNAs. (B) Total liver levels of sense strand (blue) and antisense strand (red) were quantified by RT-PCR. (C) Sense strand (blue) and antisense strand (red) levels bound to Ago2 quantified by RT-PCR. Mean  $\pm$  standard deviations are plotted ( $n = 3$  per group).

respectively. Mice were treated subcutaneously with 1 mg/kg of siRNA and evaluated on day 5 (Figure S2). Total liver levels and Ago2 loading were significantly lower for siRNA XVII than for either III and IV; however, the mRNA reductions at day 5 were indistinguishable from the more stable siRNAs. Thus, the detrimental impact of removing PS linkages from the 3' end of the GalNAc-conjugated antisense strand may not be apparent at the mRNA level until later time points, which were not collected in this experiment. The lower liver levels and Ago2 loading strongly suggest that the GalNAc ligand does not sufficiently protect the 3' terminus of the antisense strand from nuclease-mediated degradation due to the overhang structure and that the duration of action is reduced unless the 3' terminus of the antisense strand is stabilized with PS linkages.

**DNA Is Tolerated in the 3' Overhang when the 3' End of the Antisense Strand Is Conjugated to GalNAc.** Next, we investigated the impact of replacing the two 2'-OMe RNA residues in the 3' overhang in the antisense strand with DNA with either phosphodiester (IX) or PS (X) linkages (Table 1). Mice were treated subcutaneously with 1 or 2.5 mg/kg siRNA, and circulating TTR protein levels were analyzed at 7, 14, 21, and 28 days postdose. At the lower 1 mg/kg dose, siRNAs II and X had similar efficacy and duration of action (Figure 6). A maximum reduction in TTR protein of approximately 75% was observed on day 7, and TTR levels recovered to baseline at 28 days postdose. siRNA IX was of considerably lower potency and had a shorter duration with a maximum reduction of only 30% at day 7 and a return to baseline levels by day 14. At the higher 2.5 mg/kg dose, siRNA IX remained a poor performer with only 40% target knockdown on day 7 and return to baseline by day 14 (Figure 6). Interestingly, at the 2.5 mg/kg dose, both siRNA X and siRNA II resulted in barely detectable levels of TTR on day 7, but siRNA X was more potent than siRNA II at each of the following time points. These results indicate that the 3' overhang of the GalNAc-conjugated antisense strand can be DNA as long as the linkages are

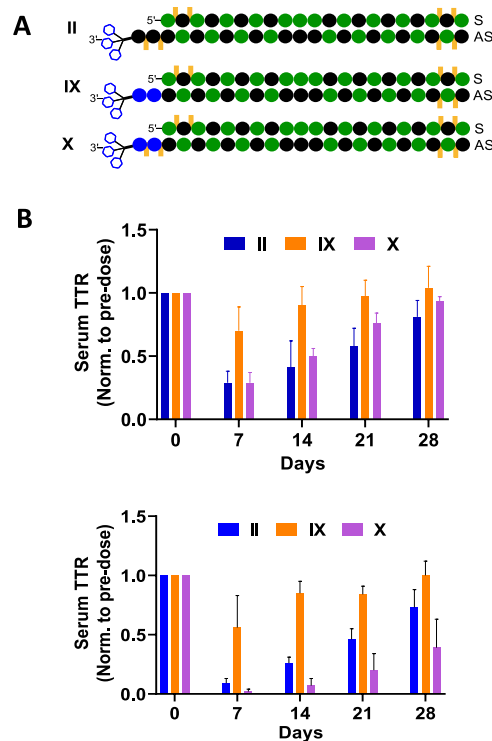


**Figure 6.** A GalNAc-conjugated antisense strand with a 3' DNA overhang with PS linkages has a long duration of action in vivo. (A) Bead diagram of tested siRNAs. (B) Serum TTR protein quantified by ELISA in mice treated with 1 mg/kg (upper) or 2.5 mg/kg (lower) siRNA II (blue), IX (orange), and X (violet) and normalized relative to predose TTR levels. Means  $\pm$  standard deviations are plotted ( $n = 3$  per group).

stabilized with PS. This design, at the higher dose, had an improved duration of action relative to the siRNA in which the

GalNAc-conjugated antisense strand terminated with two 2'-OMe residues with PS linkages.

### GalNAc Conjugation to the Antisense Strand Allows Shortening of the Antisense Strand and Increasing the Antisense Strand Length Compromises RNAi Activity.

The 5' terminus of the sense strand and the 3' terminus of the antisense strand of the siRNA interact with the PAZ domain of Ago2.<sup>21,24</sup> Most siRNAs used clinically have a 21-mer sense strand and a 23-mer antisense strand. The 23-mer antisense strand is metabolized by the loss of the 3'-terminal residue to a 22-mer, which is active in vivo.<sup>9</sup> In order to determine how GalNAc conjugation to the 3' terminus of the antisense strand influences the optimal strand lengths, we compared siRNA II, which has a 21-mer sense strand and a 23-mer antisense strand, to siRNA XI, in which both strands are 22-mers, siRNA XII, in which the sense strand is a 22-mer and an antisense strand is a 23-mer, siRNA XIII, in which both strands are 21-mers, and siRNA XIV, in which the sense strand is a 21-mer and the antisense strand is a 22-mer (Table 1). Mice were given 1 and 2.5 mg/kg doses of each siRNA subcutaneously, and TTR protein was quantified on days 7, 14, 21, 28, and 42. Differences were more apparent at the 1 mg/kg dose than at the 2.5 mg/kg dose, and siRNA XIV had the best activity of the five compounds evaluated (Figure 7A–C). The analogue of XII with terminal PS linkages in the sense strand was not tested.

Next, we assessed the impact of increasing the antisense strand to 25 nucleotides based on the speculation that there is potential for a steric clash between GalNAc or its linker with the PAZ domain of Ago2 when it is attached to the 3' end of the antisense strand. A ligand that is cleavable would remove the possibility of such a clash but may alter the oligonucleotide stability and inherent activity and duration. Two siRNAs with 25-nucleotide antisense strands resulting in four-nucleotide overhangs were synthesized (Table 1). In siRNA XV, the two PS linkages are adjacent to the duplex region and two dT nucleotides were introduced to extend the length of the overhang. In siRNA XVI, the two dT residues with PS linkages are at the terminus. siRNA XV had minimal activity at 1 mg/kg (Figure 7D), which could be due to the loss of the GalNAc ligand in circulation. siRNA XVI, which has overhang nucleotides stabilized with PS linkages, was active, although its potency was lower than that of siRNA II (Figure 7D). These results indicate that alterations of the siRNA in the region that interacts with the Ago2 PAZ domain impact siRNA potency and duration of action. Variations could be related to differences in oligonucleotide stability, interactions with Ago2, or both, but optimal activity was observed for the GalNAc conjugated antisense strand of 22 nucleotides.

**3'-Terminal GalNAc Does Not Interfere with Binding to the Ago PAZ Domain.** We used fluorescently labeled RNA hairpins to evaluate the interaction between the 3' terminus of the antisense strand with the Ago2 PAZ domain. Hairpins were synthesized that were modified with FAM in the loop region and with 3'-terminal nucleotides of UUU (as in the antisense strand modified with GalNAc) or with UUu, uuu, or UXX, where U is a deoxy U, u is 2'-OMe U, and X is a 2'-deoxy abasic residue (Figure S3A). The hairpin concentration was 10 nM, well below the  $K_d$  of 76 nM for the transition between the RNA hairpin and duplex (Figure S3B). The hairpin with the terminal UUU had a  $K_d$  of 15 nM for the purified PAZ domain (Figure S3C). Replacing the 3'-terminal nucleotide with 2'-OMe had virtually no effect; the  $K_d$  was 12

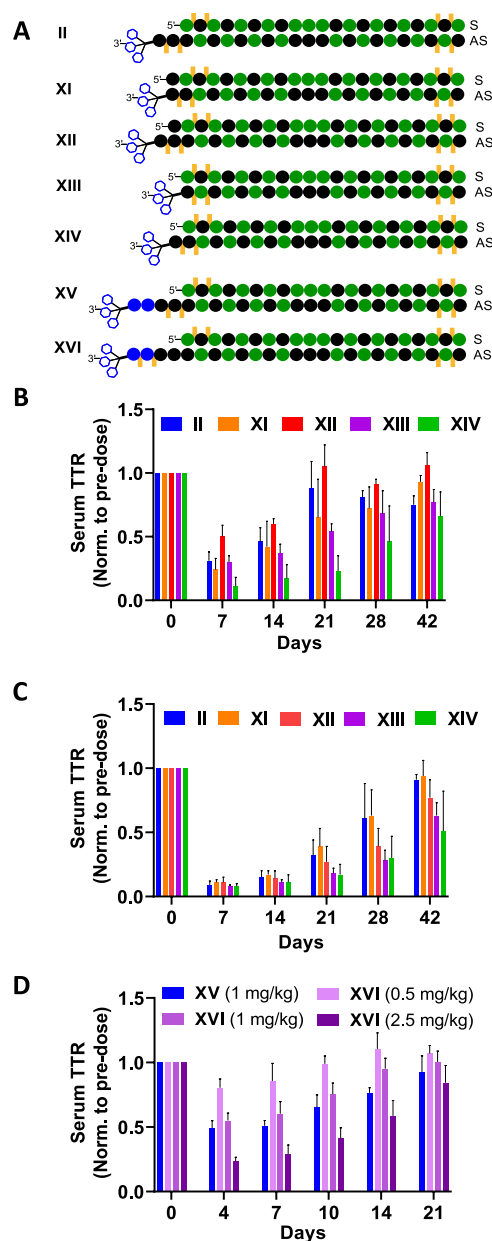


**Figure 7.** Length of the antisense strand influences both the potency and duration in vivo. (A) Bead diagram of tested siRNAs. (B, C) Serum TTR protein quantified by ELISA in mice treated with (B) 1 mg/kg or (C) 2.5 mg/kg for siRNA II (blue), XI (orange), XII (red), XIII (violet), and XIV (green). (D) Serum TTR protein was quantified by ELISA in mice treated with siRNA XV (1 mg/kg, in blue) or siRNA XVI (0.5, 1, 2.5 mg/kg in light violet, violet, and dark violet, respectively). Data were normalized to pre-dose TTR levels, and mean  $\pm$  standard deviations are plotted ( $n = 3$ ).

nM (Figure S3D). Replacing all three terminal nucleotides with 2'-OMe weakened the  $K_d$  to 40 nM (Figure S3E). Interestingly, when the two terminal Us were replaced with 2'-deoxy abasic residues, the stability of the complex changed very little as the  $K_d$  was 28 nM (Figure S3F). This showed that the binding of the 3' terminus of the antisense strand involves mainly the phosphate groups and is dominated by electrostatic interactions. Thus, replacing the 3'-terminal nucleotide by a hydroxyproline moiety that serves to attach the GalNAc conjugate via a C12 linker to the 3' end of the antisense siRNA should minimally alter the stability of the PAZ-RNA complex,

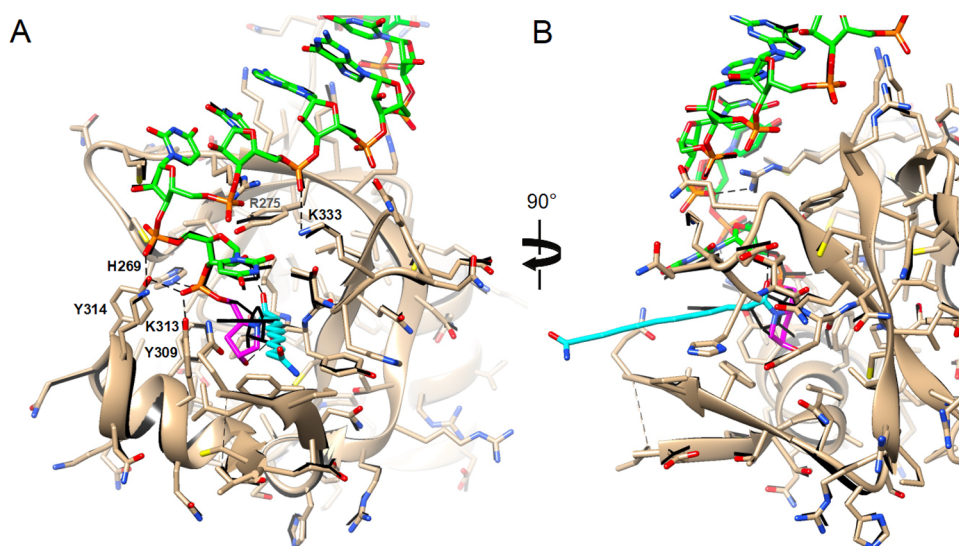


**Figure 8.** Computational model of PAZ domain bound to an RNA carrying a 3'-terminal prolinol moiety attached to a C12 linker, which is used for GalNAc conjugation. (A) The complex viewed approximately along the direction of the C12 linker, which is in an all-*trans* conformation. (B) View of the complex rotated by 90° around the vertical axis relative to the view in panel A. Carbon atoms of RNA, PAZ domain, hydroxyprolinol, and C12 linker are colored in green, beige, magenta, and cyan, respectively, and the native PAZ-RNA complex is overlaid with solid black bonds and ribbons. The two terminal phosphates are in a tight grip by His-269, Tyr-309, and Tyr-314 (the last phosphate), and Lys-313 (penultimate phosphate). These correspond to His-271, Tyr-311, His-316, and Arg-315, in Ago2 PAZ. See Figure S4 for an overlay of the Ago1 and Ago2 PAZ domains in complex with siRNA carrying a 3'-terminal prolinol moiety attached to the C12 linker. The two preceding phosphates are also engaged in salt bridges (Arg-275 and Lys-333). In addition, the model shows that the 2'-hydroxyl group of the penultimate ribose can form a hydrogen bond to the amide moiety that connects the prolinol moiety and C12 linker; the hydroxyl group of prolinol is hydrogen bonded to the main chain oxygen of Tyr-336. Salt bridges and hydrogen bonds are drawn with dashed lines.

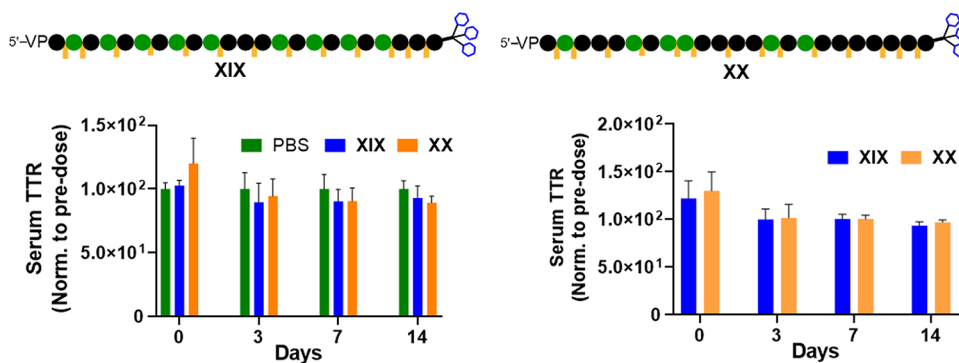


**Figure 9.** GalNAc-conjugated single-stranded siRNA targeting *Ttr* shows little activity. Upper: Bead diagrams of tested single-stranded siRNAs. Lower: Mice were treated with 3 mg/kg (left) or 10 mg/kg (right) siRNA XIX (blue) or XX (orange), and serum TTR protein was quantified by ELISA and normalized relative to predose TTR levels. Means  $\pm$  standard deviations are plotted ( $n = 3$ ).

which is what our *in vitro* and *in vivo* analyses of silencing indicate.

To further interrogate the interaction between the 3' terminus of the antisense strand and the PAZ domain, we built a model of PAZ in complex with an RNA that features a 3'-terminal hydroxyproline and a C12 linker with a terminal amide moiety. The model is based on the crystal structure of PAZ bound to a single-stranded RNA<sup>26</sup> and was energy-minimized using AMBER with ff14 force field parameters as implemented in UCSF Chimera.<sup>29</sup> The model shows that the linker attached to the prolinol moiety is outside the PAZ binding pocket on the protein surface and does not form contacts with PAZ main or side chain atoms (Figure 8 and Movie S1). Thus, the structural model is consistent with the finding that conjugation of a GalNAc to the 3' end of the antisense strand of an siRNA does not interfere with RNAi activity.

### Single-Stranded SiRNA Conjugates Do Not Function Effectively *In Vitro* or *In Vivo*.

The activity of the siRNAs with antisense strands conjugated to GalNAc raised the question of whether a single-stranded antisense siRNA that is able to target the liver could be developed. Literature precedence exists for functional single-strand siRNAs.<sup>30–34</sup> We designed two single-stranded antisense strands that target *Ttr* conjugated on the 3' end to GalNAc and fully modified with 2'-OME and 2'-fluoro (2'-F). These oligonucleotides were also modified with 5' vinylphosphonate, which has been shown to enhance stability and increase RISC loading by improving antisense strand-Ago2MID domain interactions.<sup>28,30–37</sup> Single-stranded siRNA XIX had 13 PS linkages and siRNA XX had 14 PS linkages (Table 1). In our hands, both had poor activity in the cell-based assay with IC<sub>50</sub> values of 120 and 65 nM, respectively, compared to 0.04 nM for siRNA II (Tables 1 and S2, Figure S2). In mice treated with

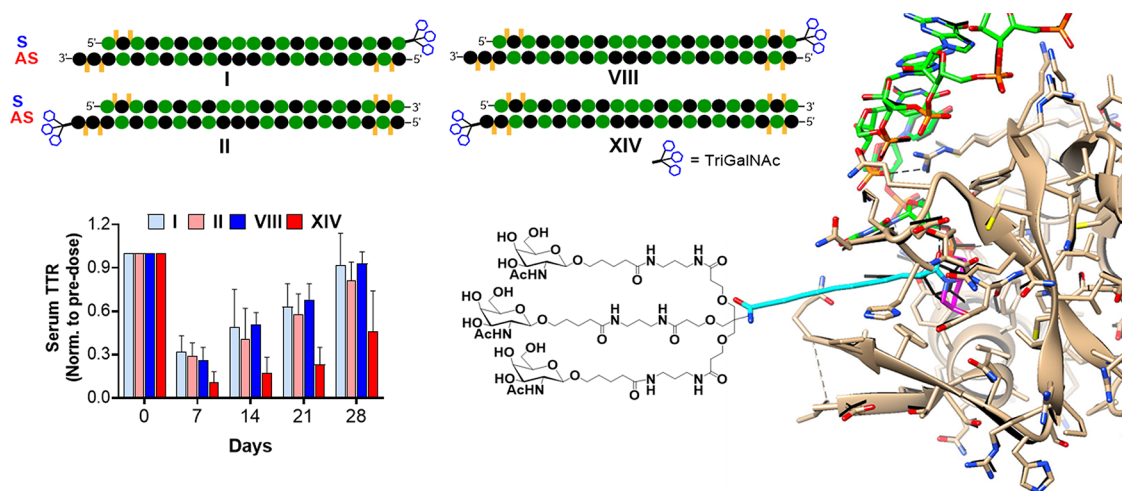


**Figure 10.** Summary of activities of siRNAs with GalNAc conjugated to the 3' end of the sense strand with 6 or 8 PS linkages (siRNAs I and VIII, respectively) and with GalNAc conjugated to the 3' end of the antisense strand (siRNA II and XIV) (1 mg/kg subcutaneous dose) along with molecular modeling rationale for the latter.

the single-stranded siRNAs, no significant reduction in serum TTR levels was observed, even at a subcutaneous dose of 10 mg/kg (Figure 9). In the original report on single-stranded siRNAs, much higher doses were employed to evaluate in vivo efficacy using different molecular targets, and the strands were not conjugated to GalNAc.<sup>30</sup> These results suggest that single-stranded oligonucleotides do not mediate RNAi at doses of up to 10 mg/kg.

## DISCUSSION

Trivalent GalNAc conjugation results in the delivery of siRNAs and other oligonucleotide therapeutics into hepatocytes, enabling the successful treatment of a variety of diseases. All approved siRNAs that are conjugated to GalNAc have the ligand at the 3' end of the sense strand.<sup>6,7,10–13,15,38,39</sup> Since our initial results published in 2014 where we demonstrated the utility of the 3' end of the sense strand, the 5' end of the sense strand has been explored. Surprisingly, conjugation to the antisense strand, which mediates recognition of the targeted mRNA, has not been pursued as it was reasoned that a ligand at the 3' end of the antisense strand would have unfavorable interactions with the PAZ domain of Ago2. Conjugation at the 3' end of an oligonucleotide, which involves the use of a GalNAc building block on solid support, is more economical than conjugation to the 5' terminus, which necessitates high concentrations of the phosphoramidite to ensure efficient coupling. The only evaluation of the conjugation of GalNAc to the antisense strand's 3' terminus was under in vitro conditions.<sup>24</sup> The 3'-terminal chemical modifications that have been evaluated in animal models were designed to improve specificity rather than to enable receptor targeting and were small compared to the large GalNAc-type targeting ligands.<sup>18–23</sup>

Here, we demonstrated that siRNAs in which the 3' terminus of the antisense strand is conjugated to triantennary GalNAc through a hydroxyprolinol linker are as potent in cell culture and in mice as siRNAs in which the conjugation to GalNAc is on the 3' end of the sense strand. This observation was confirmed by targeting three mRNAs, *Ttr*, *C5*, and *FXII*. We showed that activities correlated with in vivo liver exposures and RISC loading.

We also explored the effects of the 3' terminal chemical modifications and the length of the antisense strand on potency. With GalNAc at the 3' terminus of the antisense strand, comparable activities were observed for 3' terminal DNA or 2'-OMe residues. In crystal structures of Ago PAZ, the two 3'-terminal residues of ribonucleotide or 2'-OMe oligonucleotides adopt C3'-endo pucker (North; PDB ID 1si3 and 3mj0, respectively); in contrast, these residues of a deoxyoligonucleotide adopt the C2'-endo or C1'-exo pucker (South; PDB ID 1si2).<sup>26</sup> In mice, we found that activity was optimal when the two terminal linkages were phosphorothioate (Figure 6). This is in line with the expected protection against exonuclease degradation afforded by the PS modification, irrespective of the chemistry of the 3'-overhang. Interestingly, at the higher dose of 2.5 mg/kg, siRNA X was more potent than siRNA II, which has a PS-protected 2'-OMe overhang, throughout the course of the experiment (Figure 6B). We had expected that the 2'-OMe overhang would further improve metabolic stability. It is possible that 2'-OMe modifications at the 3' terminus of the antisense strand lowered the affinity for the PAZ domain compared with the parent ribonucleotides, although a 2'-deoxy overhang also negatively affects the affinity.<sup>26</sup> It is also possible that the 2'-OMe overhang does not interact with the PAZ domain but rather pairs with the target mRNA and hampers product release, reducing potency. Finally, it is possible that the 2'-deoxy overhang, which cannot form 2'-OH-mediated hydrogen bonds with PAZ residues seen with RNA in the crystal structures, enhances the flexibility of the antisense strand terminus and facilitates accommodation of the linker region of the GalNAc conjugate, whereas the more sterically demanding 2'-OMe overhang limits flexibility.

Previous work has shown that the 23-mer antisense strand is often degraded in vivo to yield a 22-nucleotide, active metabolite.<sup>40</sup> This complicates pharmacokinetic studies and bioanalytics of the drug substance. Therefore, we evaluated an siRNA with a GalNAc-conjugated 22-mer antisense strand. This siRNA was more potent than the parent siRNA with a 23-mer antisense strand. In contrast, lengthening the antisense strand did not provide an advantage, nor did a design with no overhang. The observation that a 21-mer sense/22-mer antisense siRNA was optimal warrants further investigation, as shortening this strand by a single nucleotide would reduce

the bioanalytical burden. Furthermore, it is worth pointing out that the 21-mer sense/22-mer antisense construct was superior to siRNAs formed from two strands of the same length, which may relate to how Ago2 recognizes the siRNA in the PAZ domain.

Ago2 appears to have a preference for 22-nucleotide antisense RNAs as most microRNAs are 22 nucleotides long.<sup>41,42</sup> Dicer and Drosha produce a duplex with a two-nucleotide overhang, and we suspect that the prolinol region of the linker of the GalNAc-conjugated antisense strand mimics the second phosphate of the natural double overhang and perhaps the second nucleobase of the overhang. Modeling of the complex between the PAZ domain of Ago2 and an oligonucleotide with a 3' hydroxyprolinol attached to a C12 linker rationalized our finding that a GalNAc ligand can be conjugated to the antisense strand of an siRNA without loss of potency. In the model, the phosphate of the hydroxyprolinol interacts favorably with the PAZ domain, and the C12 linker lies outside the oligonucleotide binding pocket. Thus, the large trivalent GalNAc ligand does not perturb interactions of the siRNA antisense strand with PAZ.

Representations of siRNAs with GalNAc conjugated to the 3' end of the sense strand (siRNA I with the conventional 6PS and VIII with 8 PS) and to the 3' end of the antisense strand (siRNA II and XIV) together with relative activities are shown in Figure 10. The latter group showed either equivalent or better potencies in mice [treated subcutaneously with 1 mg/kg of siRNA I (light blue), II (light red), VIII (blue), and XIV (red)]. Clearly, the 21/22 construct XIV with 8 PS and GalNAc at the 3' end of the antisense strand is superior to the 21/23 analogue as well as conventional GalNAc conjugated siRNAs I and VIII.

We also evaluated the activity of single-stranded siRNAs with a 3'-terminal GalNAc, a 5' vinylphosphonate, and phosphorothioate linkages for metabolic stability. These siRNAs did not induce silencing of *Ttr* in mice at the highest dose tested of 10 mg/kg, 10-fold higher than the dose at which double-stranded siRNAs were active, suggesting that the double-stranded siRNA design is vital for RNAi-mediated silencing.

## CONCLUSIONS

In this work, we carried out a systematic evaluation of siRNAs with the 3' termini of the siRNA antisense strands conjugated to GalNAc through the same hydroxyprolinol-tris scaffold-linker system used in the conjugation of 3' termini of sense strands of clinically approved siRNAs. The siRNAs with GalNAc-conjugated antisense strands had similar GalNAc-ASGPR receptor affinity and in vitro and in vivo activities and similar levels of loading into liver tissue and the RNA-induced silencing complex as siRNAs with a GalNAc-conjugated sense strand. With GalNAc at the 3' terminus of the antisense strand, comparable knockdown activities were observed for 3' terminal DNA, RNA or 2'-OME- RNA residues as long as the two terminal linkages were phosphorothioates. An siRNA with a GalNAc-conjugated antisense strand of 22 nucleotides had better activity than an siRNA with a 23-nucleotide antisense strand. This design warrants clinical evaluation, as it would simplify metabolite profiling of siRNA therapeutic agents. Computational modeling of a complex between a GalNAc-conjugated antisense strand and the PAZ domain of Ago2 demonstrated that the 3'-terminal nucleotide by the hydroxyproline moiety that serves to attach the GalNAc

conjugate via a C12 linker to the 3' end of the antisense siRNA should minimally alter the stability of the PAZ-RNA complex, rationalizing the equivalent potencies of siRNAs with GalNAc-conjugated antisense strands and siRNAs with GalNAc-conjugated sense strands. Interestingly a GalNAc-conjugated antisense single strand was not active even with extensive stabilization and 5'-VP. Our findings indicate that ligands other than GalNAc should be tested at the 3' end of antisense strands. Finally, as the targeting ligand and the pharmacophore-containing functional strand are in the same strand, the understanding of the pharmacokinetic and pharmacodynamic properties of siRNA drugs will be made simpler with this novel design.<sup>38,40,43,44</sup>

## EXPERIMENTAL SECTION

**siRNA Synthesis.** Acetonitrile was purchased from EMD Chemicals. Oligonucleotides were synthesized on an ABI 394 Synthesizer with Sterling solvents and reagents, 500-Å CPG solid supports, and 2'-deoxy, 2'-OME, and 2'-F phosphoramidites purchased from ChemGenes and used as received (all monomers had the purity level of >95%). A solution of 0.25 M 5-(*S*-ethylthio)-1*H*-tetrazole in acetonitrile was used as the activator. The phosphoramidite solutions were prepared at a concentration of 0.15 M in anhydrous acetonitrile. The oxidizing reagent was 0.02 M I<sub>2</sub> in THF/pyridine/H<sub>2</sub>O. *N,N*-Dimethyl-*N'*-(3-thioxo-3*H*-1,2,4-dithiazol-5-yl)methanimidamide, 0.1 M in pyridine, was used as the sulfurizing reagent. The detritylation reagent was 3% dichloroacetic acid in dichloromethane. After completion of the automated synthesis, the solid support was washed with 0.1 M piperidine in acetonitrile for 10 min and then washed with anhydrous acetonitrile and dried with argon. Oligonucleotides were manually deprotected using a mixture of 30% NH<sub>4</sub>OH/absolute ethanol (3:1, v/v; 0.5 mL/μmol of solid support) for 6 h at 55 °C. The solvent containing oligonucleotide was collected by filtration and stored at -20 °C prior to purification.

The crude oligonucleotides were purified by anion-exchange HPLC on an AKTA Purifier-100 chromatography system using an AP-1 glass column (10 × 200 mm, Waters) custom-packed with the DNA TSK-Gel Super Q-5PW support (TOSOH Bioscience). The desired product was purified to >85% using a linear gradient of 0.22 to 0.42 M NaBr in 0.02 M sodium phosphate, pH 8.5/15% (v) acetonitrile over 120–150 min at room temperature and then desalted by size exclusion chromatography on an AKTA Prime chromatography system using an AP-2 glass column (20 × 300 mm, Waters) custom-packed with Sephadex G25 (GE Healthcare) eluted with sterile nuclease-free water.

Oligonucleotides were analyzed by ion-exchange HPLC using a Thermo DNAPac Pa200 analytical column (4 mm × 250 mm). Buffer A was 0.025 M Tris-HCl, pH 8, 1 mM EDTA in 15% CH<sub>3</sub>CN, and buffer B was buffer A plus 1 M NaBr in 15% CH<sub>3</sub>CN. A gradient of 25 to 56% B over 21.5 min at a flow rate of 1.0 mL/min was used. The column temperature was 75 °C. Oligonucleotides were also analyzed by LC/ESI-MS on a Waters XBridge C8 column (2.1 mm × 50 mm, 2.5 μm). Buffer A was 95 mM 1,1,1,3,3,3-hexafluoro-2-propanol/16 mM triethylamine in water, and buffer B was 100% methanol. A gradient from 2% to 29% B over 26.8 min with a flow rate of 0.25 mL/min was employed. The column temperature was 60 °C. The oligonucleotide sequences and chemical modification and mass spectroscopy data are summarized in Table S1.

To generate siRNA duplexes, equimolar amounts of purified complementary strands were mixed to a final concentration of 20 μM in PBS, at pH 7.4, heated in a water bath at 95 °C for 5 min, and cooled to room temperature over a period of approximately 12 h. The siRNA duplexes met the purity criteria set by regulatory agencies and were free from all endotoxins.

**Analysis of siRNA Binding to ASGPR.** The binding of siRNAs to ASGPR was evaluated using a previously described flow cytometry-based competitive binding assay.<sup>25,45</sup> In brief, viable plateable primary mouse (CD-1) cryopreserved hepatocytes (ThermoFisher) were

resuspended at 1 million cells per mL in Dulbecco's Modified Eagle Medium (DMEM, Life Technologies) with 2% bovine serum albumin (BSA, Sigma-Aldrich). A GalNAc-conjugated, Alexa647-labeled siRNA described previously<sup>9</sup> was diluted to a final concentration of 20 nM and was premixed with the siRNA to be evaluated at concentrations from 3  $\mu$ M to 1.4 nM in DMEM with 2% BSA. To the siRNA solution were added 100,000 hepatocytes, and samples were incubated at 4 °C for 15 min. Cells were washed twice with Dulbecco's Phosphate-Buffered Saline with magnesium and calcium (DPBS, Life Technologies) with 2% BSA. Cells were suspended in a solution of DPBS with 2% BSA and 2  $\mu$ g/mL propidium iodide and analyzed on an LSRII flow cytometer (BD Biosciences). Compensation was performed using Diva software (BD Biosciences). Hepatocytes were gated by size using forward and side scatter and dead cells stained with propidium iodide were excluded from the analysis. The median fluorescent intensity of the GalNAc-conjugated, Alexa647-labeled siRNA was quantified. Data were analyzed by using FlowJo and GraphPad Prism.

**In Vitro Analysis of Gene Silencing.** A protocol from a recent publication was followed for analysis of gene silencing in cell culture.<sup>46</sup> Primary mouse hepatocytes were transfected by adding 5.0  $\mu$ L of a mixture containing Lipofectamine RNAiMax (Invitrogen, cat. no. 13778-150) and Opti-MEM plus (mixture composed of 0.1  $\mu$ L of Lipofectamine and 5.0  $\mu$ L of Opti-MEM plus) to each well, along with 5  $\mu$ L of the desired siRNA duplex into a 384-well plate and incubated at room temperature for 15 min. About 40  $\mu$ L of BioIVT Invitropro CP Rodent Medium  $\sim 5 \times 10^3$  cells was then added to the siRNA mixture. Cells were incubated for 24 h at 37 °C and then processed for RNA purification. RNA was isolated using an automated protocol on a BioTek-EL406 platform using DYNABEADS (Invitrogen, cat # 61012). Briefly, 70  $\mu$ L of Lysis/Binding Buffer and 10  $\mu$ L of Lysis/Binding Buffer containing 3  $\mu$ L of magnetic beads were added to each well. Plates were incubated on an electromagnetic shaker for 10 min at room temperature; then, magnetic beads were captured, and the supernatant was removed. Bead-bound RNA was then washed two times with 150  $\mu$ L of Wash Buffer A and once with Wash Buffer B. Beads were then washed with 150  $\mu$ L of Elution Buffer, recaptured, and supernatant removed. Next, 12  $\mu$ L of a master mix containing 1.2  $\mu$ L of 10 $\times$  Buffer, 0.48  $\mu$ L of 25 $\times$  dNTPs, 1.2  $\mu$ L of 10 $\times$  Random primers, 0.6  $\mu$ L of Reverse Transcriptase, 0.6  $\mu$ L of RNase inhibitor, and 7.92  $\mu$ L of water per reaction was added to the RNA. Plates were sealed, mixed, and incubated on an electromagnetic shaker for 10 min at room temperature, followed by 2 h at 37 °C. Aliquots of 2  $\mu$ L of cDNA were added to a master mix containing 2  $\mu$ L of water, 0.5  $\mu$ L of either an appropriate GAPDH TaqMan VIC Probe or the target probe, and 5  $\mu$ L of Lightcycler 480 probe master mix (Roche, cat no. 04887301001) per well in a 384 well plate (Roche, cat # 04887301001). Real-time PCR was performed in a LightCycler480 Real-Time PCR system (Roche). Each duplex was tested in quadruplicate and data were normalized to cells transfected with a nontargeting control siRNA. To calculate relative fold change, real-time data were analyzed using the  $\Delta\Delta$ Ct method and normalized to assays performed with cells transfected with a nontargeting control siRNA.

**In Vivo Evaluation of siRNA-Mediated Silencing.** In vivo experiments were conducted in 6–8 week-old female C57BL/6 or Balb/c mice acquired from Charles River Laboratories. All studies were conducted at Alnylam Pharmaceuticals in accordance with animal procedures reviewed and approved by the Institutional Animal Care and Use Committee. Animals were administered siRNA or PBS (Gibco) via a subcutaneous injection. Animals were sacrificed at time points ranging from 1 to 28 days postdose.

Livers were harvested and snap-frozen for analysis of the hepatic mRNA of interest. Total RNA was isolated using the QIAzol reagent (Qiagen) or using the Qiagen RNeasy kit. RNA concentrations were determined by using a Nanodrop spectrophotometer (ThermoFisher Scientific). The RNA concentrations were adjusted to 25 ng/ $\mu$ L, and cDNA was synthesized from 250 ng of a sample using a reverse transcription kit from Applied Biosystems. RT-PCR was employed for

RNA quantification as described in the section on analysis of in vitro activity.

Blood was collected by utilizing the retro-orbital eye bleed procedure at selected time points to assess levels of proteins of interest. For this procedure, the mice were anesthetized using isoflurane. Heparin-coated capillary tubes (Fisher Scientific) were inserted into the posterior corner of the mouse eye; the tube was inserted at a 45° angle to approximately 1 cm and rotated until the blood from the retro-orbital sinus was released. Approximately 200  $\mu$ L was collected from the left eye of each mouse according to the IACUC protocol for blood collection. The blood was collected in Becton Dickinson serum separator tubes. Serum samples obtained for analysis of proteins other than C5 were kept at room temperature for 1 h and then spun in a microcentrifuge at 22  $\times$  g at room temperature for 10 min. The serum was transferred to 1.5 mL microcentrifuge tubes for storage at –80 °C until samples were processed.

For analysis of serum TTR levels, serum samples were diluted 1:4000 and assayed using an ELISA (ALPCO, catalog number 41-PALMS-E01). Protein concentrations were determined by comparison to a TTR standard prepared in-house.

**Evaluation of In Vivo RISC Loading and Liver Levels of siRNA.** In vivo RISC loading was evaluated according to a published procedure.<sup>28</sup> Ago2-bound siRNA from mouse liver was quantified by preparing liver powder lysates at 100 mg/mL in 50 mM Tris–HCl, pH 7.5, 150 mM NaCl, 2 mM EDTA, and 0.5% Triton-X 100 supplemented with freshly added protease inhibitors (Sigma-Aldrich, P8340) at 1:100 dilution and 1 mM PMSF (Life Technologies). Total liver lysate (10 mg) was used for each Ago2 immunoprecipitation and control immunoprecipitation. Anti-Ago2 antibody was purchased from Wako Chemicals (Clone No.: 2D4). Control mouse IgG was obtained from Santa Cruz Biotechnology (sc-2025). Protein G Dynabeads (Life Technologies) were used to precipitate the antibodies. Ago2-associated siRNAs were eluted by heating in 50  $\mu$ L PBS, 0.25% Triton (95 °C, 5 min) and quantified by stem-loop RT-qPCR as described previously.<sup>47,48</sup>

Determination of liver levels of siRNA-GalNAc conjugates was performed according to a previously published procedure.<sup>49</sup> Mice were sacrificed on day 5 (for TTR and C5 experiments) postdose, and livers were snap-frozen in liquid nitrogen and ground into powder. Total siRNA liver levels were measured by reconstituting liver powder at 10 mg/mL in PBS containing 0.25% Triton-X 100. The tissue suspension was ground with 5 mm steel grinding balls at 50 cycles/s for 5 min in a tissue homogenizer (Qiagen TissueLyser LT) at 4 °C. Homogenized samples were then heated at 95 °C for 5 min, briefly vortexed, and allowed to rest on ice for 5 min. Samples were then centrifuged at 21,000  $\times$  g for 5 min at 4 °C. The siRNA sense and antisense strand levels in supernatants were quantified by stem-loop RT-qPCR as previously described.<sup>47,48</sup>

**Fluorescence-Based  $K_d$  Measurements for Ago2 PAZ-RNA Complexes.** To measure the effect of modifications at the two 3'-terminal uridines of the antisense strand on PAZ binding, we prepared FAM-modified RNA hairpins of the sequence 5'-ACA GUG GYU CCA CUG UUU-3', where Y is dT-FAM and loop nucleotides are highlighted by italics, and the 3'-terminal nucleotides were UUU (native), UUu, uuu, and UXX, where U is deoxy U, u is 2'-OMe U, and X is a 2'-deoxy abasic residue as described.<sup>50</sup> The Ago2 PAZ domain, residues 227 to 352, was expressed as a fusion protein with an N-terminal cleavable His-6 tag and purified by nickel affinity chromatography. The His tag was removed by incubation with PreScission protease, and the PAZ domain fragment was further purified using Q and S fast-flow Sepharose column chromatography and by passage through GST and Ni columns. Steady-state techniques were employed to monitor changes in the FAM fluorescence emission intensity at 516 nm. Titrations of the native and 3'-modified RNA hairpins with the PAZ domain were performed using a Fluorolog ISA Jobin Yvon-Spex spectrometer. The temperature of the cell compartment was kept at 20 °C by using a refrigerated circulating water bath. The hairpin concentration was 10 nM, and the PAZ domain concentration was increased from 2 and 250 nM. All measurements were corrected for dilution and blank solutions. Fluorescence

emission data served as input for GraphPad Prism (version 5.00 for Mac, Graph-Pad Software). Nonlinear regression in combination with the equation for “one site-specific binding” was used to compute  $K_d$  values for RNA hairpin-PAZ complexes.

**Modeling of GalNAc-Conjugated RNA Bound to the Ago2 PAZ Domain.** Coordinates of the complex between the PAZ domain and the RNA nonamer 5'-CGU GAC UCU-3' were retrieved from the Protein Data Bank (PDB ID 1si3).<sup>26</sup> The 3'-penultimate C was changed to U and the 3'-terminal U was replaced by a prolinol moiety in UCSF Chimera.<sup>29</sup> The C12 amide linker for the GalNAc conjugate was added in an all-*trans* conformation using the Structure Editing “Build Structure” option in Tools. The PAZ-RNA complex model was energy-minimized using the Amber ff 14SB force field as implemented in UCSF Chimera. Both steepest descent and conjugate gradient type minimizations were performed until convergence was reached as judged by no further resulting geometric changes. All illustrations were generated using the program UCSF Chimera.

## ■ ASSOCIATED CONTENT

### SI Supporting Information

The Supporting Information is available free of charge at <https://pubs.acs.org/doi/10.1021/acs.jmedchem.4c02250>.

siRNA oligonucleotide sequences and analytical characterizations; siRNA oligonucleotide sequences and chemical modifications, affinities for ASGPR, and potencies under transfection and free uptake conditions; evaluation of silencing in mice for C-5 mRNA; activities of single-stranded siRNAs in vitro; fluorescence-based  $K_d$  measurements for Ago2 PAZ-RNA complexes; and evaluation of complexes between PAZ and siRNA carrying a 3'-terminal GalNAc linker (PDF)

Modeled complex between PAZ and siRNA carrying a 3'-terminal linker (MP4)

## ■ AUTHOR INFORMATION

### Corresponding Author

Muthiah Manoharan – *Alnylam Pharmaceuticals, Cambridge, Massachusetts 02142, United States*; [orcid.org/0000-0002-7931-1172](https://orcid.org/0000-0002-7931-1172); Phone: +1-617-551-8319; Email: [mmanoharan@alnylam.com](mailto:mmanoharan@alnylam.com)

### Authors

Rajat S. Das – *Alnylam Pharmaceuticals, Cambridge, Massachusetts 02142, United States*; [orcid.org/0000-0003-3169-6218](https://orcid.org/0000-0003-3169-6218)  
Dhrubajyoti Datta – *Alnylam Pharmaceuticals, Cambridge, Massachusetts 02142, United States*  
Christopher R. Brown – *Alnylam Pharmaceuticals, Cambridge, Massachusetts 02142, United States*  
Jason A. Gilbert – *Alnylam Pharmaceuticals, Cambridge, Massachusetts 02142, United States*  
Amy Chan – *Alnylam Pharmaceuticals, Cambridge, Massachusetts 02142, United States*  
Jennifer Willoughby – *Alnylam Pharmaceuticals, Cambridge, Massachusetts 02142, United States*  
Swati Gupta – *Alnylam Pharmaceuticals, Cambridge, Massachusetts 02142, United States*  
MaryBeth Kim – *Alnylam Pharmaceuticals, Cambridge, Massachusetts 02142, United States*  
Rohan Degaonkar – *Alnylam Pharmaceuticals, Cambridge, Massachusetts 02142, United States*  
Tim Racie – *Alnylam Pharmaceuticals, Cambridge, Massachusetts 02142, United States*

Li Lei – *Department of Biochemistry and Center for Structural Biology, Vanderbilt University, School of Medicine, Nashville, Tennessee 37232-0146, United States*

Mark K. Schlegel – *Alnylam Pharmaceuticals, Cambridge, Massachusetts 02142, United States*; [orcid.org/0000-0002-0127-608X](https://orcid.org/0000-0002-0127-608X)

Adam Castoreno – *Alnylam Pharmaceuticals, Cambridge, Massachusetts 02142, United States*

Klaus Charisse – *Alnylam Pharmaceuticals, Cambridge, Massachusetts 02142, United States*

Kallanthottathil G. Rajeev – *Alnylam Pharmaceuticals, Cambridge, Massachusetts 02142, United States*; [orcid.org/0000-0002-0104-0237](https://orcid.org/0000-0002-0104-0237)

Martin Egli – *Department of Biochemistry and Center for Structural Biology, Vanderbilt University, School of Medicine, Nashville, Tennessee 37232-0146, United States*; [orcid.org/0000-0003-4145-356X](https://orcid.org/0000-0003-4145-356X)

Complete contact information is available at:

<https://pubs.acs.org/10.1021/acs.jmedchem.4c02250>

## Notes

The authors declare no competing financial interest.

## ■ ACKNOWLEDGMENTS

We dedicate this work to Professor Alexander Rich for his contributions to the study of structure and function of DNA, RNA and Proteins on the occasion of his centennial birthday celebrations (15 November 1924). We thank Professor David Bartel for helpful discussions.

## ■ ABBREVIATIONS

2'-F	2'-fluoro
2'-OMe	2'-O-methyl
Ago2	Argonaute 2
AMBER	Assisted Model Building with Energy Refinement
ASGPR	asialoglycoprotein receptor
GalNAc	tri- <i>N</i> -acetylgalactosamine
PS	phosphorothioate
RNAi	RNA interference
RT-PCR	Reverse transcription polymerase chain reaction
RT-qPCR	Quantitative reverse transcription polymerase chain reaction
siRNAs	small interfering RNA
mTTR	mouse TTR
Ttr	Transthyretin protein
TTR	Transthyretin gene
VP	5' vinylphosphonate

## ■ REFERENCES

- (1) Egli, M.; Manoharan, M. Re-Engineering RNA Molecules into Therapeutic Agents. *Acc. Chem. Res.* **2019**, *52*, 1036–1047.
- (2) Shen, X.; Corey, D. R. Chemistry, mechanism and clinical status of antisense oligonucleotides and duplex RNAs. *Nucleic Acids Res.* **2018**, *46*, 1584–1600.
- (3) Setten, R. L.; Rossi, J. J.; Han, S.-P. The current state and future directions of RNAi-based therapeutics. *Nat. Rev. Drug Discovery* **2019**, *18*, 421–446.
- (4) Bumcrot, D.; Manoharan, M.; Koteliansky, V.; Sah, D. W. Y. RNAi therapeutics: a potential new class of pharmaceutical drugs. *Nat. Chem. Biol.* **2006**, *2*, 711–719.
- (5) Roberts, T. C.; Langer, R.; Wood, M. J. A. Advances in oligonucleotide drug delivery. *Nat. Rev. Drug Discovery* **2020**, *19*, 673–694.

- (6) Liebow, A.; Li, X.; Racie, T.; Hettinger, J.; Bettencourt, B. R.; Najafian, N.; Haslett, P.; Fitzgerald, K.; Holmes, R. P.; Erbe, D.; et al. An Investigational RNAi Therapeutic Targeting Glycolate Oxidase Reduces Oxalate Production in Models of Primary Hyperoxaluria. *J. Am. Soc. Nephrol.* **2017**, *28*, 494–503.
- (7) Chan, A.; Liebow, A.; Yasuda, M.; Gan, L.; Racie, T.; Maier, M.; Kuchimanchi, S.; Foster, D.; Milstein, S.; Charisse, K.; et al. Preclinical Development of a Subcutaneous ALAS1 RNAi Therapeutic for Treatment of Hepatic Porphyrias Using Circulating RNA Quantification. *Mol. Ther. Nucleic Acids* **2015**, *4*, No. e263.
- (8) Fitzgerald, K.; White, S.; Borodovsky, A.; Bettencourt, B. R.; Strahs, A.; Clausen, V.; Wijngaard, P.; Horton, J. D.; Taubel, J.; Brooks, A.; et al. A Highly Durable RNAi Therapeutic Inhibitor of PCSK9. *N. Engl. J. Med.* **2017**, *376*, 41–51.
- (9) Nair, J. K.; Willoughby, J. L. S.; Chan, A.; Charisse, K.; Alam, M. R.; Wang, Q.; Hoekstra, M.; Kandasamy, P.; Kel'in, A. V.; Milstein, S.; et al. Multivalent N-Acetylgalactosamine-Conjugated siRNA Localizes in Hepatocytes and Elicits Robust RNAi-Mediated Gene Silencing. *J. Am. Chem. Soc.* **2014**, *136*, 16958–16961.
- (10) Khvorova, A. Oligonucleotide Therapeutics — A New Class of Cholesterol-Lowering Drugs. *N. Engl. J. Med.* **2017**, *376*, 4–7.
- (11) Ray, K. K.; Landmesser, U.; Leiter, L. A.; Kallend, D.; Dufour, R.; Karakas, M.; Hall, T.; Troquay, R. P. T.; Turner, T.; Visseren, F. L. J.; et al. Inclisiran in Patients at High Cardiovascular Risk with Elevated LDL Cholesterol. *N. Engl. J. Med.* **2017**, *376*, 1430–1440.
- (12) Sheridan, C. PCSK9-gene-silencing, cholesterol-lowering drug impresses. *Nat. Biotechnol.* **2019**, *37*, 1385–1387.
- (13) Kosmas, C. E.; Estrella, A. M.; Sourlas, A.; Silverio, D.; Hilario, E.; Montan, P. D.; Guzman, E. Inclisiran: a new promising agent in the management of hypercholesterolemia. *Diseases* **2018**, *6*, 63.
- (14) Springer, A. D.; Dowdy, S. F. GalNAc-siRNA Conjugates: Leading the Way for Delivery of RNAi Therapeutics. *Nucleic Acid Ther.* **2018**, *28*, 109–118.
- (15) Liu, A.; Zhao, J.; Shah, M.; Migliorati, J. M.; Tawfik, S. M.; Bahal, R.; Rasmussen, T. P.; Manautou, J. E.; Zhong, X.-B. Nedosiran, a Candidate siRNA Drug for the Treatment of Primary Hyperoxaluria: Design, Development, and Clinical Studies. *ACS Pharmacol. Transl. Sci.* **2022**, *5*, 1007–1016.
- (16) Kumar, V.; Turnbull, W. B. Targeted delivery of oligonucleotides using multivalent protein-carbohydrate interactions. *Chem. Soc. Rev.* **2023**, *52*, 1273–1287.
- (17) Kamiya, Y.; Takai, J.; Ito, H.; Murayama, K.; Kashida, H.; Asanuma, H. Enhancement of Stability and Activity of siRNA by Terminal Substitution with Serinol Nucleic Acid (SNA). *ChemBioChem* **2014**, *15*, 2549–2555.
- (18) Maiti, M.; Nauwelaerts, K.; Lescrinier, E.; Herdewijn, P. Structural and binding study of modified siRNAs with the Argonaute 2 PAZ domain by NMR spectroscopy. *Chemistry* **2011**, *17*, 1519–1528.
- (19) Valenzuela, R. A.; Onizuka, K.; Ball-Jones, A. A.; Hu, T.; Suter, S. R.; Beal, P. A. Guide Strand 3'-End Modifications Regulate siRNA Specificity. *ChemBioChem* **2016**, *17*, 2340–2345.
- (20) Alagia, A.; Jorge, A. F.; Aviñón, A.; Cova, T. F. G. G.; Crehuet, R.; Grijalvo, S.; Pais, A. A. C. C.; Eritja, R. Exploring PAZ/3'-overhang interaction to improve siRNA specificity. A combined experimental and modeling study. *Chemical Science* **2018**, *9*, 2074–2086.
- (21) Nawale, G. N.; Bahadorikhalili, S.; Sengupta, P.; Kadekar, S.; Chatterjee, S.; Varghese, O. P. 4'-Guanidinium-modified siRNA: a molecular tool to control RNAi activity through RISC priming and selective antisense strand loading. *Chem. Commun.* **2019**, *55*, 9112–9115.
- (22) Neumeier, J.; Meister, G. siRNA Specificity: RNAi Mechanisms and Strategies to Reduce Off-Target Effects. *Front. Plant Sci.* **2021**, *11*, No. 526455.
- (23) Davis, S. M.; Sousa, J.; Vangjeli, L.; Hassler, M. R.; Echeverria, D.; Knox, E.; Turanov, A. A.; Alterman, J. F.; Khvorova, A. 2'-O-Methyl at 20-mer Guide Strand 3' Termini May Negatively Affect Target Silencing Activity of Fully Chemically Modified siRNA. *Mol. Ther. - Nucleic Acids* **2020**, *21*, 266–277.
- (24) Weingärtner, A.; Bethge, L.; Weiss, L.; Sternberger, M.; Lindholm, M. W. Less Is More: Novel Hepatocyte-Targeted siRNA Conjugates for Treatment of Liver-Related Disorders. *Mol. Ther. - Nucleic Acids* **2020**, *21*, 242–250.
- (25) Severgnini, M.; Sherman, J.; Sehgal, A.; Jayaprakash, N. K.; Aubin, J.; Wang, G.; Zhang, L.; Peng, C. G.; Yucius, K.; Butler, J.; et al. A rapid two-step method for isolation of functional primary mouse hepatocytes: cell characterization and asialoglycoprotein receptor based assay development. *Cytotechnology* **2012**, *64*, 187–195.
- (26) Ma, J. B.; Ye, K.; Patel, D. J. Structural basis for overhang-specific small interfering RNA recognition by the PAZ domain. *Nature* **2004**, *429*, 318–322.
- (27) Elkayam, E.; Kuhn, C.-D.; Tocilj, A.; Haase, A. D.; Greene, Emily M.; Hannon, G. J.; Joshua-Tor, L. The Structure of Human Argonaute-2 in Complex with miR-20a. *Cell* **2012**, *150*, 100–110.
- (28) Elkayam, E.; Parmar, R.; Brown, C. R.; Willoughby, J. L.; Theile, C. S.; Manoharan, M.; Joshua-Tor, L. siRNA carrying an (E)-vinylphosphonate moiety at the 5' end of the guide strand augments gene silencing by enhanced binding to human Argonaute-2. *Nucleic Acids Res.* **2017**, *45*, 3528–3536.
- (29) Pettersen, E. F.; Goddard, T. D.; Huang, C. C.; Couch, G. S.; Greenblatt, D. M.; Meng, E. C.; Ferrin, T. E. UCSF Chimera—a visualization system for exploratory research and analysis. *J. Comput. Chem.* **2004**, *25*, 1605–1612.
- (30) Lima, W. F.; Prakash, T. P.; Murray, H. M.; Kinberger, G. A.; Li, W.; Chappell, A. E.; Li, C. S.; Murray, S. F.; Gaus, H.; Seth, P. P.; et al. Single-Stranded siRNAs Activate RNAi in Animals. *Cell* **2012**, *150*, 883–894.
- (31) Li, Z.; Wang, X.; Zhou, X.; Wang, J.; Guan, Z.; Yang, Z. Optimization in Chemical Modification of Single-Stranded siRNA Encapsulated by Neutral Cytidiny/Cationic Lipids. *Front. Chem.* **2022**, *10*, No. 843181.
- (32) Yu, D.; Pendergraft, H.; Liu, J.; Kordasiewicz, H. B.; Cleveland, D. W.; Swayze, E. E.; Lima, W. F.; Crooke, S. T.; Prakash, T. P.; Corey, D. R. Single-Stranded RNAs Use RNAi to Potently and Allele-Selectively Inhibit Mutant Huntingtin Expression. *Cell* **2012**, *150*, 895–908.
- (33) Dorsett, Y.; Tuschl, T. J. siRNAs: applications in functional genomics and potential as therapeutics. *Nat. Rev. Drug Discovery* **2004**, *3*, 318–329.
- (34) Prakash, T. P.; Lima, W. F.; Murray, H. M.; Elbashir, S.; Cantley, W.; Foster, D.; Jayaraman, M.; Chappell, A. E.; Manoharan, M.; Swayze, E. E.; et al. Lipid Nanoparticles Improve Activity of Single-Stranded siRNA and Gapmer Antisense Oligonucleotides in Animals. *ACS Chem. Biol.* **2013**, *8*, 1402–1406.
- (35) Parmar, R. G.; Brown, C. R.; Matsuda, S.; Willoughby, J. L. S.; Theile, C. S.; Charisse, K.; Foster, D. J.; Zlatev, I.; Jadhav, V.; Maier, M. A.; et al. Facile Synthesis, Geometry, and 2'-Substituent-Dependent in Vivo Activity of 5'-(E)- and 5'-(Z)-Vinylphosphonate-Modified siRNA Conjugates. *J. Med. Chem.* **2018**, *61*, 734–744.
- (36) Prakash, T. P.; Lima, W. F.; Murray, H. M.; Li, W.; Kinberger, G. A.; Chappell, A. E.; Gaus, H.; Seth, P. P.; Bhat, B.; Crooke, S. T.; et al. Identification of metabolically stable 5'-phosphate analogs that support single-stranded siRNA activity. *Nucleic Acids Res.* **2015**, *43*, 2993–3011.
- (37) Schirle, N. T.; Kinberger, G. A.; Murray, H. F.; Lima, W. F.; Prakash, T. P.; MacRae, I. J. Structural Analysis of Human Argonaute-2 Bound to a Modified siRNA Guide. *J. Am. Chem. Soc.* **2016**, *138*, 8694–8697.
- (38) An, G. Pharmacokinetics and Pharmacodynamics of GalNAc-Conjugated siRNAs. *J. Clin. Pharmacol.* **2024**, *64*, 45–57.
- (39) Egli, M.; Manoharan, M. Chemistry, structure and function of approved oligonucleotide therapeutics. *Nucleic Acids Res.* **2023**, *51*, 2529–2573.
- (40) McDougall, R.; Ramsden, D.; Agarwal, S.; Agarwal, S.; Aluri, K.; Arciprete, M.; Brown, C.; Castellanos-Rizaldos, E.; Charisse, K.; Chong, S.; et al. The Nonclinical Disposition and Pharmacokinetic/

Pharmacodynamic Properties of N-Acetylgalactosamine-Conjugated Small Interfering RNA Are Highly Predictable and Build Confidence in Translation to Human. *Drug. Metab. Dispos.* **2022**, *50*, 781–797.

(41) Ambros, V.; Bartel, B.; Bartel, D. P.; Burge, C. B.; Carrington, J. C.; Chen, X.; Dreyfuss, G.; Eddy, S. R.; Griffiths-Jones, S.; Marshall, M.; et al. A uniform system for microRNA annotation. *RNA* **2003**, *9*, 277–279.

(42) Zhang, H.; Kolb, F. A.; Jaskiewicz, L.; Westhof, E.; Filipowicz, W. Single processing center models for human Dicer and bacterial RNase III. *Cell* **2004**, *118*, 57–68.

(43) Kandasamy, P.; Mori, S.; Matsuda, S.; Erande, N.; Datta, D.; Willoughby, J. L. S.; Taneja, N.; O’Shea, J.; Bisbe, A.; Manoharan, R. M.; et al. Metabolically Stable Anomeric Linkages Containing GalNAc-siRNA Conjugates: An Interplay among ASGPR, Glycosidase, and RISC Pathways. *J. Med. Chem.* **2023**, *66*, 2506–2523.

(44) Debacker, A. J.; Voutila, J.; Catley, M.; Blakey, D.; Habib, N. Delivery of Oligonucleotides to the Liver with GalNAc: From Research to Registered Therapeutic Drug. *Mol. Ther.* **2020**, *28*, 1759–1771.

(45) Matsuda, S.; Keiser, K.; Nair, J. K.; Charisse, K.; Manoharan, R. M.; Kretschmer, P.; Peng, C. G.; Kel’in, V. A.; Kandasamy, P.; Willoughby, J. L. S.; et al. siRNA Conjugates Carrying Sequentially Assembled Trivalent N-Acetylgalactosamine Linked Through Nucleosides Elicit Robust Gene Silencing In Vivo in Hepatocytes. *ACS Chem. Biol.* **2015**, *10*, 1181–1187.

(46) Schlegel, M. K.; Matsuda, S.; Brown, C. R.; Harp, J. M.; Barry, J. D.; Berman, D.; Castoreno, A.; Schofield, S.; Szeto, J.; Manoharan, M.; et al. Overcoming GNA/RNA base-pairing limitations using isonucleotides improves the pharmacodynamic activity of ESC +GalNAc-siRNAs. *Nucleic Acids Res.* **2021**, *49*, 10851–10867.

(47) Pei, Y.; Hancock, P. J.; Zhang, H.; Bartz, R.; Cherrin, C.; Innocent, N.; Pomerantz, C. J.; Seitzer, J.; Koser, M. L.; Abrams, M. T.; et al. Quantitative evaluation of siRNA delivery in vivo. *RNA* **2010**, *16*, 2553–2563.

(48) Chen, C.; Ridzon, D. A.; Broomer, A. J.; Zhou, Z.; Lee, D. H.; Nguyen, J. T.; Barbisin, M.; Xu, N. L.; Mahuvakar, V. R.; Andersen, M. R.; et al. Real-time quantification of microRNAs by stem-loop RT-PCR. *Nucleic Acids Res.* **2005**, *33*, No. e179.

(49) Nair, J. K.; Attarwala, H.; Sehgal, A.; Wang, Q.; Aluri, K.; Zhang, X.; Gao, M.; Liu, J.; Indrakanti, R.; Schofield, S.; et al. Impact of enhanced metabolic stability on pharmacokinetics and pharmacodynamics of GalNAc-siRNA conjugates. *Nucleic Acids Res.* **2017**, *45*, 10969–10977.

(50) Kumar, P.; Parmar, R. G.; Brown, C. R.; Willoughby, J. L. S.; Foster, D. J.; Babu, I. R.; Schofield, S.; Jadhav, V.; Charisse, K.; Nair, J. K.; et al. 5'-Morpholino modification of the sense strand of an siRNA makes it a more effective passenger. *Chem. Commun.* **2019**, *55*, 5139–5142.